

# Strain-Tuned Incompatible Magnetic Exchange-Interaction in $\text{La}_2\text{NiO}_4$

Izabela Bialo,<sup>1,2,\*</sup> Leonardo Martinelli,<sup>1</sup> Gabriele De Luca,<sup>3</sup> Paul Worm,<sup>4</sup> Annabella Drewanowski,<sup>1</sup> Simon Jöhr,<sup>1</sup> Jaewon Choi,<sup>5</sup> Mirian Garcia-Fernandez,<sup>5</sup> Stefano Agrestini,<sup>5</sup> Ke-Jin Zhou,<sup>5</sup> Kurt Kummer,<sup>6</sup> Nicholas B. Brookes,<sup>6</sup> Luo Guo,<sup>7</sup> Anthony Edgeton,<sup>7</sup> Chang B. Eom,<sup>7</sup> Jan M. Tomczak,<sup>8,4</sup> Karsten Held,<sup>4</sup> Marta Gibert,<sup>4</sup> Qisi Wang,<sup>9,1,†</sup> and Johan Chang<sup>1</sup>

<sup>1</sup>Physik-Institut, Universität Zürich, Winterthurerstrasse 190, CH-8057 Zürich, Switzerland

<sup>2</sup>AGH University of Krakow, Faculty of Physics and Applied Computer Science, 30-059 Krakow, Poland

<sup>3</sup>Institut de Ciència de Materials de Barcelona (ICMAB-CSIC), 08193 Bellaterra (Barcelona), Spain

<sup>4</sup>Institute of Solid State Physics, Vienna University of Technology, A-1040 Vienna, Austria

<sup>5</sup>Diamond Light Source, Harwell Campus, Didcot, Oxfordshire OX11 0DE, United Kingdom

<sup>6</sup>ESRF, The European Synchrotron, 71 Avenue des Martyrs, CS40220, 38043 Grenoble Cedex 9, France

<sup>7</sup>Department of Materials Science and Engineering,

University of Wisconsin-Madison, Madison, 53706, Wisconsin, USA

<sup>8</sup>Department of Physics, King's College London, Strand, London WC2R 2LS, United Kingdom

<sup>9</sup>Department of Physics, The Chinese University of Hong Kong, Shatin, Hong Kong, China

## Abstract

Magnetic frustration is a route for novel ground states, including spin liquids and spin ices. Such frustration can be introduced through either lattice geometry or incompatible exchange interactions. Here, we find that epitaxial strain is an effective tool for tuning antiferromagnetic exchange interactions in a square-lattice system. By studying the magnon excitations in  $\text{La}_2\text{NiO}_4$  films using resonant inelastic x-ray scattering, we show that the magnon displays substantial dispersion along the antiferromagnetic zone boundary, at energies that depend on the lattice of the film's substrate. Using first principles simulations and an effective spin model, we demonstrate that the antiferromagnetic next-nearest neighbour coupling is a consequence of the two-orbital nature of  $\text{La}_2\text{NiO}_4$ . Altogether, we illustrate that compressive epitaxial strain enhances this coupling and, as a result, increases the level of incompatibility between exchange interactions within a model square-lattice system.

## Introduction

The square-lattice Heisenberg model is the subject of intense numerical and experimental investigations. In spin-1/2 systems—such as cuprates [1] and copper deuterioformate tetradeurate (CFTD) [2]—higher-order exchange interactions are inferred from observations of magnon dispersions along the magnetic zone boundary [3, 4]. While a detailed magnon characterization is useful to understand quantum-fluctuation effects [? ], exchange incompatibility is typically avoided in these systems. Indeed, the antiferromagnetic (AF) nearest-neighbor (NN) exchange interaction ( $J_1 > 0$ ) and the ferromagnetic next-nearest-neighbour (NNN) interaction ( $J_2 < 0$ ) in these

systems stabilize the classical AF Néel order. Instead, magnetic exchange incompatibility requires both  $J_1 > 0$  and  $J_2 > 0$ . This regime of the  $J_1$ - $J_2$  model is the subject of extensive computational investigations for both spin  $S = 1/2$  [5–9] and  $S = 1$  [10, 11] systems. In a narrow range near  $J_2/J_1 \sim 1/2$ , magnetic frustration is found to dominate, and exotic quantum phases such as the spin-liquid state [12] are predicted. Several calculations show that the Néel order is destroyed there and the ground state has a valence-bond character [12–14], although its exact nature is still the subject of debate [7, 15]. However, only very few square-lattice systems exhibit substantial magnetic frustration [16, 17], and even fewer display tunable magnetic interactions [18]. As a result, approaching the interesting parameter regime in real materials remains an ongoing issue.

In this article, we provide a high resolution resonant inelastic x-ray scattering (RIXS) study of magnetic excitations in epitaxial thin films of the canonical  $S = 1$  system  $\text{La}_2\text{NiO}_4$ , grown on different substrates. We discover a marked, upward dispersion along the AF zone-boundary  $(1/2, 0) \rightarrow (1/4, 1/4)$ , which reveals the presence of AF NNN interactions that partly frustrate the NN ones. By employing *ab initio* calculations, we demonstrate that these results can only be explained by including the multi-orbital nature of  $3d^8$ -Ni systems. Furthermore, we observe a correlation between the relative strength of the magnetic interactions and the strain applied onto the films. Our results demonstrate that 214-type nickelates are a promising class of materials for the study of the AF square-lattice Heisenberg model. Moreover, the use of thin films provides a clear route to tune the magnetic frustration and explore so far inaccessible regions of the magnetic phase diagram.

## Results

Our thin films of  $\text{La}_2\text{NiO}_4$  (LNO) on  $\text{SrTiO}_3$  (STO),  $\text{LaAlO}_3$  (LAO),  $(\text{LaAlO}_3)_{0.3}(\text{Sr}_2\text{TaAlO}_6)_{0.7}$  (LSAT) and  $\text{NdGaO}_3$  (NGO) substrates are characterized by atomic force microscopy, x-ray diffraction, and x-ray absorption

\* izabela.bialo@uzh.ch

† qwang@cuhk.edu.hk

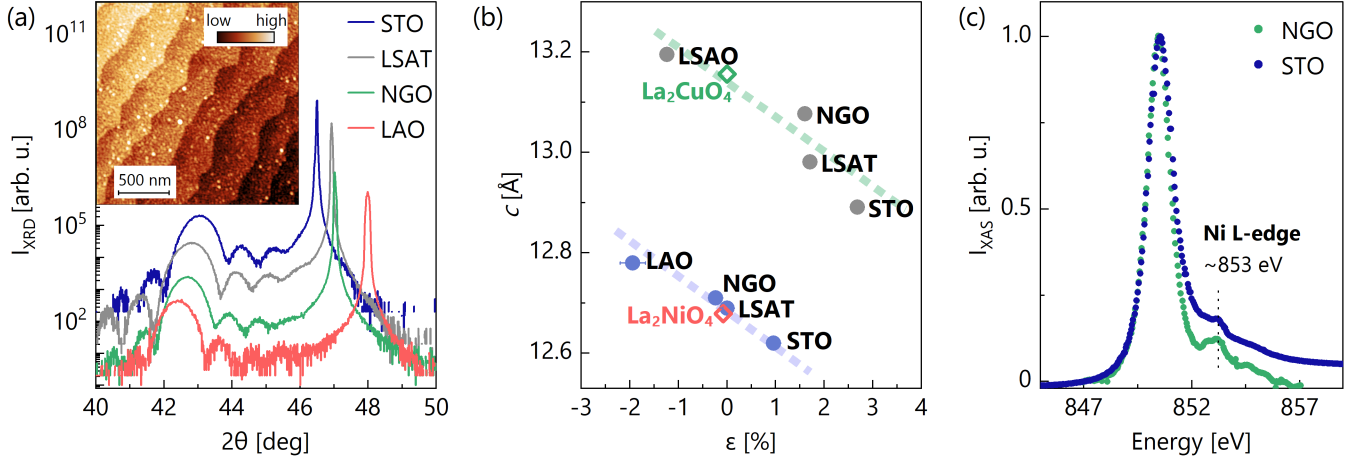


FIG. 1. **Characterization measurements on thin films of  $\text{La}_2\text{NiO}_4$ .** (a) X-ray diffraction (at 300 K) probing the  $(0, 0, \ell)$  direction of 12 nm thin films of  $\text{La}_2\text{NiO}_4$  on substrates as indicated. The inset represents the atomic force microscopy image showing the step-like morphology of the films (here for the NGO substrate). The color scale corresponds to film thickness. (b)  $c$ -axis lattice parameter versus in-plane epitaxial strain (at 300 K) calculated for  $\text{La}_2\text{NiO}_4$  (purple dots) and  $\text{La}_2\text{CuO}_4$  [19] (gray dots) films grown on different substrates as a relative change of in-plane parameters in reference to bulk (diamonds) with  $a = 3.868 \text{ \AA}$  and  $c = 12.679 \text{ \AA}$  for an isomorphous  $\text{La}_2\text{NiO}_4$  structure [20] and  $a = 3.803 \text{ \AA}$  and  $c = 13.156 \text{ \AA}$  for  $\text{La}_2\text{CuO}_4$  [21]. The errorbar correspond to the spread of in-plane parameters measured by x-ray diffraction. (c) X-ray absorption spectra around the Ni  $L$ -edge. The dominant peak corresponds to the La  $M$ -edge. (b,c) Dashed lines are guides to the eye.

spectroscopy – see Fig. 1. The atomic force microscopy images display a step-like morphology indicating an excellent layer-by-layer growth. Diffraction patterns probing the  $(0, 0, \ell)$  reciprocal direction demonstrate good single crystallinity and allow us to extract the  $c$ -axis lattice parameters of the films. The epitaxial strain applied by the substrates is supported by the film  $c$ -axis and in-plane lattice-parameter dependence (Fig. 1b). X-ray absorption spectra recorded on the LNO/STO and LNO/NGO, shown in Fig. 1c, are consistent with observations on related nickelates [22–25]. The Ni  $L$ -edge features on the tail of the La  $M$ -edge.

The RIXS spectra of  $\text{La}_2\text{NiO}_4$  films were measured at the Ni  $L_3$  edge (853 eV). These spectra exhibit key RIXS excitations, including high-energy  $dd$ -excitations (at approximately 0.5–3 eV), an elastic scattering contribution at 0 eV, as well as phonon and magnon excitations in between. The  $dd$ -excitations have a multi-peak structure, qualitatively similar to other  $3d^8$  systems, such as NiO [22–24, 26]. As shown in Fig. 2a, the relative intensities of the peaks are different in the three samples, due to the different crystal-fields acting on the Ni atoms (see Fig. S1, Supplementary Note 1). However, all our  $\text{La}_2\text{NiO}_4$  films display the most intense  $dd$ -excitation around 1.1 eV and a second less intense excitation just below 1.6 eV. This is consistent with what is reported in bulk  $\text{La}_2\text{NiO}_4$  [27] (see Fig. S2, Supplementary Note 1). The subtraction of the elastic peak clearly highlights the presence of multiple low-energy features; see Figs. 2b,c.

To extract the dispersion of magnetic excitations, we assumed a two-mode model with the addition of a high-energy continuum “background” (Fig. 2b,c). Each of

these components is represented by a Gaussian profile. This provides an effective fitting model of excitations for all measured film systems and momenta. Our interpretation of the proposed model is based on the hypothesis that the lower-energy mode ( $\sim 40 \text{ meV}$ ) stems from an optical phonon, while the higher-energy mode (strongly dispersing between 60 and 120 meV) is a magnon. This assignment is supported by previous neutron scattering measurements that identified the phonon part via an out-of-plane oxygen buckling mode [28, 29]. The interpretation of the higher-energy mode as a magnon is consistent with earlier RIXS [27] and neutron studies [30] of bulk  $\text{La}_2\text{NiO}_4$ . The resulting magnon dispersions are shown in Fig. 3.

Due to lower energy resolution, the previous RIXS study [27] did not resolve any phonon excitations. The unresolved phonon excitation implied that the phonon and magnon spectral weights were merged. This, in turn influences the extraction of the magnon dispersion. Having access, in this work, to a higher energy resolution, we can distinguish between the nearly momentum-independent phonon mode and the dispersive magnon branch along the three measured high-symmetry directions. In all the film systems explored, the magnon energy reaches its maximum at the AF zone boundary, at the  $\Sigma$  point  $(1/4, 1/4)$ , referred to as  $E_\Sigma$ , while it displays a local minimum at the  $X$  point  $(1/2, 0)$ , referred to as  $E_X$ . This evidently anisotropic shape of magnon dispersion was not reported in earlier studies [27, 30], except for a recent inelastic neutron scattering experiment [31]. Furthermore, the energy  $E_\Sigma$  is different for all three substrates. In particular, it

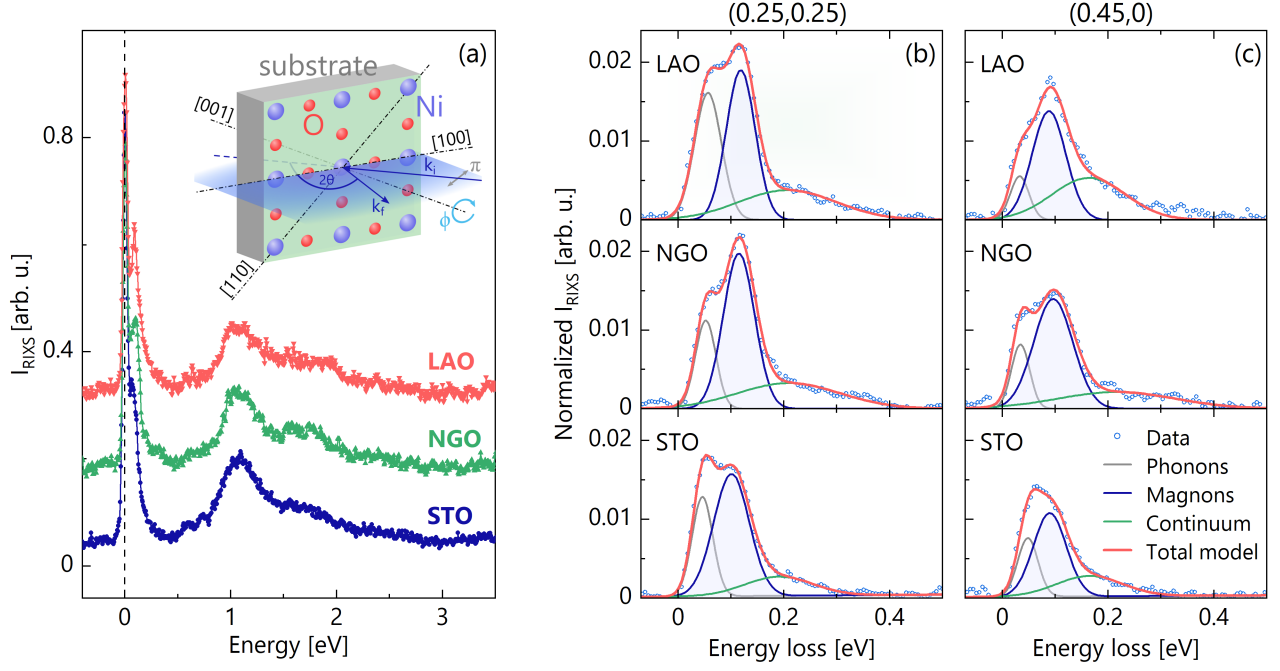


FIG. 2. **Resonant inelastic x-ray scattering spectra of  $\text{La}_2\text{NiO}_4$ .** (a) Raw spectra recorded in  $\text{La}_2\text{NiO}_4$  films with substrates as indicated. (a,inset) Schematics of the photon-in-photon-out resonant inelastic x-ray scattering (RIXS) geometry with horizontally polarized light ( $\pi$ ) and azimuthal sample rotation angle  $\phi$ . (b,c) Low-energy part of the RIXS spectra with momentum transfer and film substrates indicated. The solid red line indicates a three-component fit with phonon, magnon (shaded), and multi-magnon (continuum) contributions. The elastic scattering channel is subtracted in (b,c).

increases as a function of compressive strain, with an enhancement of  $18 \pm 4$  meV ( $\sim 20\%$ ) from LNO/STO to LNO/LAO.

### Discussion

By resolving both the phonon and magnon modes, we find that all samples exhibit a substantial dispersion of magnetic excitations along the AF zone boundary. This directly implies the presence of higher-order effective magnetic exchange interactions. In  $\text{La}_2\text{CuO}_4$  and related Mott insulating cuprates, the zone boundary dispersion has been interpreted in terms of a positive ring-exchange interaction that emerges naturally from a single-orbital Hubbard model [19, 32, 33]. There is, however, an important difference between the zone-boundary dispersion of  $\text{La}_2\text{CuO}_4$  and  $\text{La}_2\text{NiO}_4$ : in contrast to  $\text{La}_2\text{CuO}_4$ , the zone boundary dispersion of  $\text{La}_2\text{NiO}_4$  has its maximum at the AF zone boundary  $\Sigma$  point rather than at the X point. As such, the magnon dispersion of  $\text{La}_2\text{NiO}_4$  is (as could be expected) inconsistent with a single-band Hubbard model in the strong coupling limit (where the projection onto a Heisenberg spin Hamiltonian is viable).

As a first step, we parameterize the magnon dispersion of  $\text{La}_2\text{NiO}_4$  using a phenomenological spin-wave model that includes effective NN and NNN exchange interactions, respectively  $J_1$  and  $J_2$  (Fig. 3), plus an easy-plane anisotropy  $K$ , already reported by previous measurements [30, 31]. As a starting point, we employ the AF

structure of the bulk  $\text{La}_2\text{NiO}_4$  determined by neutron diffraction [34–36], with the spin direction parallel to the crystallographic  $a$ -axis. The model is solved in a linear spin-wave (large- $S$ ) limit, and the calculated dispersion is fitted to the measured one (see Methods). Fitting the experimental (exp) data yields an effective NN exchange interaction  $J_1^{\text{exp}} \sim 30$  meV consistent with previous neutron and RIXS results [27, 37]. Due to the demonstrated finite zone-boundary dispersion, our spin-wave model fitting also yields a moderate NNN exchange interaction  $J_2^{\text{exp}}$ . Importantly,  $J_2^{\text{exp}}$  is positive and enhanced by compressive strain [3, 4]. In what follows, we wish to extract the frustration parameter  $\mathcal{G} = J_2^{\text{exp}}/J_1^{\text{exp}}$  with the highest precision. Within our spin-wave model,  $E_X = 4SZ_c(J_1 - 2J_2)$  and  $E_\Sigma = 4SZ_c(J_1 - J_2)$ , where  $Z_c$  is the quantum renormalization factor for spin-wave energies, which is taken as  $Z_c = 1.09$  [38]. This gives  $\mathcal{G}^{-1} = 1 + E_\Sigma/(E_\Sigma - E_X)$ . The frustration parameter  $\mathcal{G}$  is thus derived directly from the experimental data, with high precision ( $E_\Sigma$  and  $E_X$  are extracted with error lower than 5 meV) and plotted as a function of the  $c$  lattice parameter in Fig. 4 (see also Table S1, Supplementary Note 2). Due to the Poisson effect, the  $c$  lattice parameter undergoes a proportional shrinkage when the in-plane parameters expand. Our x-ray diffraction measurements confirm this relationship (Fig. 1b), indicating that the  $c$ -axis lattice parameter can serve as an indirect probe of the in-plane strain. Therefore, our findings demonstrate

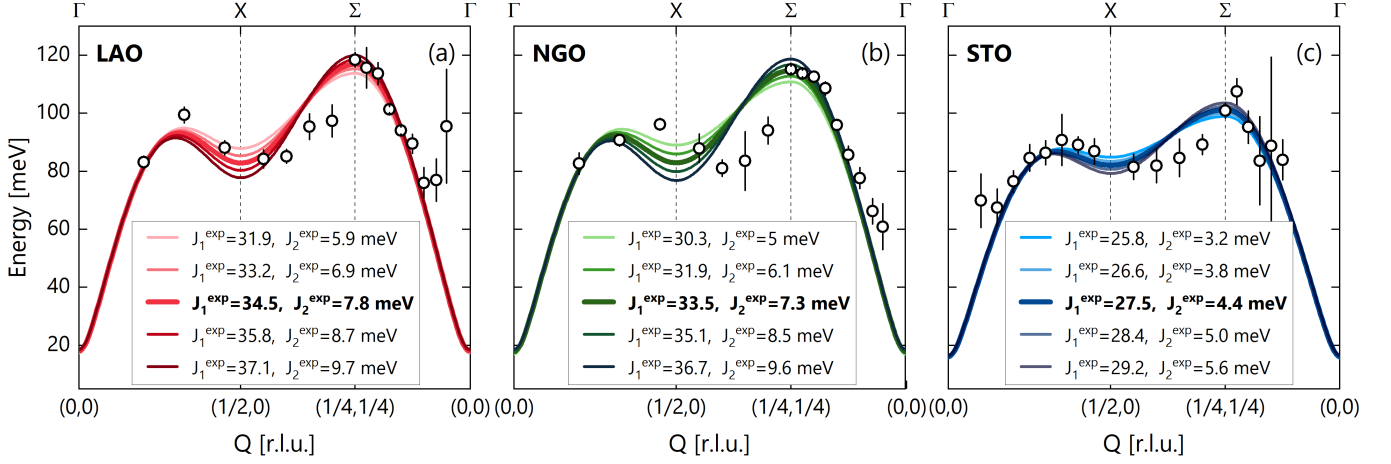


FIG. 3. **Magnon dispersion of  $\text{La}_2\text{NiO}_4$  films.** (a-c) Magnon excitation energies (open dots) along high symmetry directions for  $\text{La}_2\text{NiO}_4$  on substrates as indicated. Solid lines represent the same spin wave model evaluated for different exchange parameters within the confidence intervals of the fitted parameters. The curves corresponding to the best-fit values (marked in bold in the legend) are reported as thicker lines. The middle segment,  $X \rightarrow \Sigma$ , is part of the antiferromagnetic zone-boundary. The error bars are determined from the fitting uncertainty.

a nearly linear correlation between magnetic frustrations and epitaxial strain.

We stress that, for interaction strengths and hoppings that are realistic for cuprates and nickelates,  $J_2 > 0$  is hard to reconcile with a single-band Hubbard model. A positive  $J_2$  implies an effective AF NNN exchange interaction, at odds with what is observed in cuprates [4, 32] and  $d^9$  infinite-layer nickelates [39, 40]. Both systems have indeed been successfully described using a single  $d$ -orbital framework [3, 4, 41, 42]. Therefore, we argue that the magnon zone boundary dispersion in LNO signals physics beyond the single-orbital Hubbard model. We propose that the multi-orbital ( $d_{x^2-y^2}$ ,  $d_{z^2}$ ) nature of nickelates [43–45] must be explicitly considered. Already in  $\text{La}_2\text{CuO}_4$ , due to the short apical oxygen distance, a small but significant orbital hybridization between  $d_{z^2}$  and  $d_{x^2-y^2}$  has been reported [46]. In  $\text{La}_2\text{NiO}_4$  the apical oxygen distance is even shorter, as exemplified by the reduced  $c$  lattice parameter (see Fig. 1b), and hence an even more pronounced hybridization is expected.

To rationalize the trend in the exchange interactions obtained from our spin-wave fits, we derive a two-orbital low-energy model for  $\text{La}_2\text{NiO}_4$  on different substrates from first principles (see the Method section). For the Ni  $d_{z^2}$  and  $d_{x^2-y^2}$  orbitals (labeled  $\alpha$  and  $\beta$ ), we compute the (next) nearest-neighbor hopping parameters  $t^{(\nu)}$ , the crystal field splitting  $\Delta_{eg}$ , local Coulomb (Hubbard) interaction  $U$  and Hund’s exchange  $J_H$  using experimental lattice constants from Table I. Noteworthy[47], the hopping parameters and Coulomb interactions, listed in Table I, hardly change under varying in-plane compression. This is different from calculations for the cuprate family, see Ref. 19, and agrees with our experiments, which show substantially smaller changes in the magnon spectrum than for the cuprates. What is most affected by

strain in Table I is the crystal-field splitting  $\Delta_{eg}$  by which the Ni  $d_{x^2-y^2}$  orbital is higher in energy than the  $d_{z^2}$  orbital. When going from the STO to the LAO substrate, in-plane strain pushes the  $d_{x^2-y^2}$  orbital further up in energy, as it is pointing towards the now closer in-plane oxygen sites that are charged negatively.

This crystal-field splitting  $\Delta_{eg}$  enters the calculated (cal) two-orbital superexchange as follows:

$$J_1^{\text{cal}} = \frac{t_{\alpha\beta}^2}{U + J_H - \Delta_{eg}} + \frac{t_{\alpha\beta}^2}{U + J_H + \Delta_{eg}} + \frac{t_{\alpha\alpha}^2 + t_{\beta\beta}^2}{U + J_H}, \quad (1)$$

where we extend the formula of Ref. 48 to finite  $\Delta_{eg}$  (see Supplementary Note 3). As  $\Delta_{eg}$  appears once with a plus and once with a minus sign in the denominator, the crystal-field splitting enters  $J_1^{\text{cal}}$  in a higher-than-linear order.

The magnetic exchange couplings  $J_1^{\text{cal}}$  determined by Eq. (1) are displayed in Table I. They show the same qualitative tendency as in our experiment, i.e., an increase of both  $J_1^{\text{exp}}$  (see Fig. 3) and  $J_1^{\text{cal}}$  with compressive strain. Quantitatively, the *ab initio* calculated  $J_1^{\text{cal}}$  is however too large. This has two major origins: (i) The cRPA interactions are, here, taken at zero frequency  $U = U(\omega = 0)$ . Additional renormalizations from the frequency dependence  $U(\omega)$  [49] are often mimicked through an empirical enhancement of  $U$ . Increasing  $U$ , we could easily obtain quantitative agreement with the experimental  $J_1$ , but at the cost of a free fit parameter and most likely only an accidental agreement. (ii) Eq. (1) only includes terms to second-order perturbation theory in  $t$ . For the one-band Hubbard model, higher-order processes have been calculated and yield a correction from  $J_1 = 4t^2/U$  to a reduced  $J_1 = 4(t^2/U - 16t^4/U^3)$  [41, 50]. Higher-order terms are expected to reduce  $J_1$  also in the



System	$a$ [Å]	$c$ [Å]	$\Delta_{eg}$ [eV]	$t_{\alpha\alpha}$ [eV]	$t_{\beta\beta}$ [eV]	$t_{\alpha\beta}$ [eV]	$t'_{\alpha\alpha}$ [meV]	$t'_{\beta\beta}$ [meV]	$U_{\alpha\alpha}$ [eV]	$U_{\beta\beta}$ [eV]	$U_{\alpha\beta}$ [eV]	$J_H$ [eV]	$J_1^{\text{cal}}$ [meV]	$J_2^{\text{cal}}$ [meV]	$J_1^{\text{cal,corr}}$ [meV]
La <sub>2</sub> NiO <sub>4</sub>	3.890	12.55	0.48	-0.070	-0.403	-0.161	-8.6	74.9	3.06	3.15	1.97	0.52	60.7	1.57	51.0
LNO/STO	3.905	12.62	0.48	-0.067	-0.395	-0.156	-8.3	74.5	3.01	3.14	1.94	0.52	59.5	1.56	49.7
LNO/LSAT	3.868	12.69	0.55	-0.065	-0.410	-0.156	-7.4	76.3	3.00	3.11	1.92	0.51	62.2	1.65	51.8
LNO/NGO	3.859	12.71	0.58	-0.064	-0.414	-0.155	-7.1	76.7	3.03	3.16	1.97	0.51	62.3	1.65	51.9
LNO/LAO	3.793	12.78	0.74	-0.060	-0.447	-0.156	-5.5	80.5	3.02	3.08	1.93	0.50	71.6	1.83	56.8

TABLE I. **Parameters of the two-orbital Hubbard model.** Crystal field splitting  $\Delta_{eg}$ , (next-)nearest neighbor hopping  $t'_{ij}$  between  $i$ -th and  $j$ -th Ni orbitals ( $\alpha$  and  $\beta$  here denote the  $z^2$  and  $x^2 - y^2$  orbital, respectively), the inter- and intra-orbital Coulomb interaction  $U_{ij}$ , and Hund's exchange  $J_H$  between the two orbital as calculated by DFT and cRPA with the in-plane lattice constant  $a$  of the three substrates; note that  $t'_{\alpha\beta} = 0$  by symmetry. From these *ab initio* calculated parameters the spin couplings  $J_1$  and  $J_2$  are calculated from super-exchange (second order perturbation theory), i.e., from Eq. (1) with  $t$  and  $t'$ , respectively. Estimating higher order terms using a one-orbital analogy, yields the reduced  $J_1^{\text{cal,corr}}$  couplings – see text. The bulk lattice parameters refer to the low temperature tetragonal polymorph of La<sub>2</sub>NiO<sub>4</sub>, after Ref. 31.

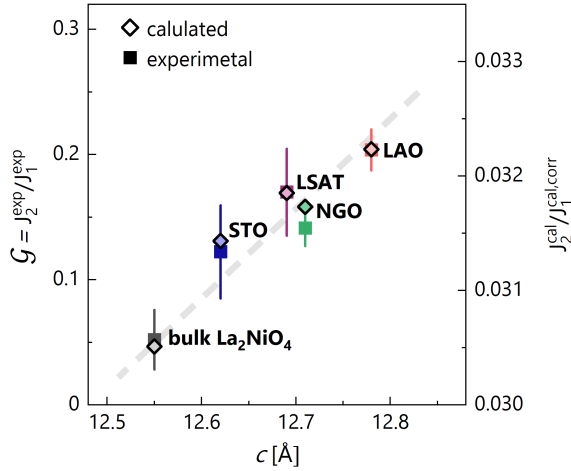


FIG. 4. **Strain dependent magnetic frustration.** The frustration parameter  $\mathcal{G} = J_2^{\text{exp}}/J_1^{\text{exp}}$  derived from the experimental data (squares; left axis) is presented as a function of the  $c$ -axis lattice parameter. The error bars for the experimental data are calculated as a propagation of standard deviations extracted from the fits. The results for films are combined with data for bulk La<sub>2</sub>NiO<sub>4</sub> from Ref. 31. The experimental frustration  $\mathcal{G}$  is compared to the ratio  $J_2^{\text{cal}}/J_1^{\text{cal,corr}}$  derived from the DFT and cRPA calculations (diamonds; right axis). Note that the calculated  $J_2^{\text{cal}}$  only contains a contribution to the full next nearest-neighbor coupling  $J_2$ . Therefore, the comparison merely highlights a similar trend of the frustration under in-plane compression. The dashed line is a guide-to-the-eye.

two-orbital setting. Here, we estimate these corrections by the one-orbital prescription  $t^2/U \rightarrow t^2/U - 16t^4/U^3$ . Then, e.g., for the NGO substrate, the leading contribution to  $J_1^{\text{cal}}$ , i.e.,  $t_{\beta\beta}^2/(U_{\text{eff}})$  with  $U_{\text{eff}} = U + J_H$ , reduces from 47 meV to 37 meV. Applying this substitution to Eq. (1) yields the corrected exchange couplings  $J_1^{\text{cal,corr}}$  listed in Tab. I, which are in better agreement with the measured values (see Fig. 3).

Table I also lists the next-nearest neighbor exchange  $J_2^{\text{cal}}$  that can be obtained with the same second-order for-

mula Eq. (1), except now using the hoppings  $t'$  instead of  $t$  (see Supplementary Note 3 for details). Crucially, our calculations predict a positive  $J_2$ , in agreement with the experiment. Moreover,  $J_2^{\text{cal}}$  shows the same qualitative tendency as in the experiment as a function of epitaxial strain. On a quantitative level, the calculated values are, however, a factor  $\sim 3 - 5$  lower than the experimental results. The reason is that contributions to  $J_2$  from higher-order exchange processes, of order  $t^4/U^3$  and  $t't^2/U^2$ , become (relatively) more important for  $J_2^{\text{cal}}$ , as the second-order terms are now based on the much smaller  $t'$ .

The key difference between the multi-orbital case of LNO and the one-orbital cuprates is the larger  $U$  ( $U_{\text{cRPA}} \approx 3.1$  eV for two-orbitals while  $U_{\text{cRPA}} \approx 1.9$  eV for a one Ni  $d_{x^2-y^2}$  orbital setup) and the additional Hund's  $J_H \approx 0.5$  eV in the denominator of Eq. (1). As a consequence, the balance for the NNN exchange coupling shifts from a ferromagnetic ring exchange  $J_2 \sim -t^4/U_{\text{eff}}^3 < 0$ , that overpowers the AF second-order exchange  $J_2 \sim t'^2/U_{\text{eff}} > 0$  in the one-orbital cuprates, toward dominance of the latter in the multi-orbital LNO. This change in hierarchy explains the main qualitative differences in magnon dispersion between LNO and cuprates: the opposite sign of the effective  $J_2$ . For LNO, with a positive  $J_2$ , the zone-boundary dispersion shows a notable minimum at  $(1/2, 0)$ , see Fig. 3, whereas a maximum occurs for the negative  $J_2$  in cuprates.

## Conclusions

The *ab-initio* calculations indicate that the magnetic frustration in La<sub>2</sub>NiO<sub>4</sub> is caused by the multi-orbital nature of  $3d^8$  nickelates. More importantly, our results demonstrate that the degree of frustration is amplified by compressive strain (see Fig. 4), with a pivotal role played by the crystal-field splitting. Indeed, with the substrates used, the magnetic frustration increases four-fold with respect to the bulk, bridging half the way toward the exotic realm anticipated for  $J_2/J_1 \sim 1/2$ . Thus, our study suggests an effective

tool for tuning antiferromagnetic interactions within square lattice systems. We speculate that the approach is applicable beyond  $\text{La}_2\text{NiO}_4$  and may offer an experimental route to reach so far unexplored regions of the magnetic phase diagram, potentially allowing to investigate exotic states induced by magnetic frustration.

## Methods

**Film growth and characterization.** Thin films of  $\text{La}_2\text{NiO}_4$  were grown by RHEED-equipped Radio-frequency off-axis magnetron sputtering [51] on (001) STO, (001) LAO, (001) LSAT and (110) NGO substrates. These films were grown in an argon atmosphere at 700°C. Their qualities were confirmed by atomic force microscopy and x-ray diffraction. Their insulating character was confirmed by resistivity measurements of the LNO/STO film (see Fig. S3, Supplementary Note 4).

**RIXS experiments.** Ni  $L$ -edge RIXS experiments for STO, LAO and NGO substrates were carried out at the I21 beamline [52] at the DIAMOND Light Source. All spectra were collected in the grazing exit geometry using linear horizontal polarized incident light with the scattering angle fixed to  $2\theta = 154^\circ$ . The energy resolution was estimated from the elastic scattering on amorphous carbon tape and was between 37-41 meV (full-width-at-half-maximum, FWHM). All films were measured at base temperature  $T = 16$  K. We define the reciprocal space  $(q_x, q_y, q_z)$  in reciprocal lattice units  $(h, k, \ell) = (q_x a/2\pi, q_y b/2\pi, q_z c/2\pi)$  where  $a, b$  and  $c$  are the pseudo-tetragonal lattice parameters. RIXS spectra were acquired along three in-plane paths:  $(0, 0) \rightarrow (0, 1/2)$ ,  $(0, 0) \rightarrow (1/4, 1/4)$  and  $(0, 1/2) \rightarrow (1/4, 1/4)$ . Extraction of low-energy excitations around  $(0, 0)$  is limited by energy resolution. Due to kinematic constraints  $\Gamma$  points at higher zones cannot be reached, as well. RIXS intensities are normalized to the weight of the  $dd$  excitations [53]. The data for the LSAT substrate were collected at the ID32 beamline at the European Synchrotron Radiation Facility (ESRF) (see description in Supplementary Note 5, Fig. S4).

**Phenomenological spin-wave model.** The effective superexchange parameters were extracted from the measured dispersion using a linear spin wave model. We included effective couplings between the first and second nearest neighbours, plus an easy-plane anisotropy  $K$ , with the resulting Hamiltonian:

$$\mathcal{H} = J_1 \sum_{\langle i, j \rangle} \mathbf{S}_i \cdot \mathbf{S}_j + J_2 \sum_{\langle\langle i, j \rangle\rangle} \mathbf{S}_i \cdot \mathbf{S}_j + K \sum_i (S_i^z)^2 \quad (2)$$

where  $\langle i, j \rangle$  and  $\langle\langle i, j \rangle\rangle$  denote pairs of first and second nearest neighbours Ni atoms, respectively. The fitting procedure has been carried out using the SpinW package [54]. As an input we have used the AF structure of the bulk  $\text{La}_2\text{NiO}_4$  determined by neutron diffraction [34–36], with the spin direction parallel to the crys-

tallographic  $a$ -axis. The dispersion in the approximation of the linear spin wave theory is represented by [4, 31]:

$$\begin{aligned} \hbar\omega &= Z_c \sqrt{(A_{\mathbf{q}}^2 - B_{\mathbf{q}}^2)} \\ A_{\mathbf{q}} &= 4S \left[ \frac{K}{4} + J_1 - J_2(1 - \nu_h \nu_k) \right] \\ B_{\mathbf{q}} &= 4S \left[ J_1 \frac{\nu_h + \nu_k}{2} - \frac{K}{4} \right] \end{aligned} \quad (3)$$

where  $\nu_x = \cos(2\pi x)$ . The quantum renormalization factor for spin-wave velocity is fixed to  $Z_c = 1.09$ , as usual for  $S = 1$  systems [38]. The value of the easy-plane anisotropy  $K$  mostly controls the size of the magnon gap at the  $\Gamma$  point. Since this value is very hard to obtain from RIXS spectra, we have fixed  $K = 0.5$  meV in agreement with previous inelastic neutron scattering data [30]. We have also neglected other interactions  $< 10^{-1}$  meV such as easy-axis anisotropy, inter-layer coupling and Dzyaloshinskii–Moriya interactions [31, 35].

**Ab initio calculations.** Electronic structure calculations were performed with density functional theory in the local density approximation using a full-potential linearized muffin-tin orbital (FPLMTO) code [55], after the structures were optimized with WIEN2k [56] using the PBE functional. We mimicked the influence of the substrates by simulating bulk  $\text{La}_2\text{NiO}_4$  using the experimental lattice constants of the thin films. The reference calculation for the bulk uses lattice constants from Ref. 31. All calculations assume the space group  $I4/mmm$  and are paramagnetic. The resulting band-structures are displayed in Fig. S5, Supplementary Note 6. The FPLMTO calculations were converged using  $12^3$  reducible  $k$ -points and include local orbitals for the Ni-3p and La-5p states. The internal atomic positions were relaxed with WIEN2k using  $6^3$  reducible  $k$ -points, a cutoff parameter RMTKMAX = 7 and partial waves inside the atomic spheres up to  $l = 5$ , until the forces were below 1mRy per Bohr radius (for details of the relaxed structures, see Supplementary Note 7, Table S2). The tight-binding hopping and crystal-field parameters have been extracted from a projection onto maximally localized Wannier orbitals [57, 58] of Ni  $3d_{x^2-y^2}$  and  $3d_{z^2}$  character. Matrix elements of the static ( $\omega = 0$ ) and local screened Coulomb interaction (Hubbard  $U$  and Hund's  $J_H$ ) have been estimated from calculations in the constrained random phase approximation (cRPA) [49] for entangled band-structures [59] in the Wannier basis [58] using  $6 \times 6 \times 6$  reducible momentum-points in the Brillouin zone. For the two-particle product basis, states are kept up to an angular cutoff of  $l = 4$  and down to an overlap eigenvalue of  $10^{-4}$ .

## Data availability

Data supporting the findings of this study are available from corresponding authors upon reasonable request.

### Code availability

Code supporting the data processing of this study is available from corresponding authors upon reasonable request.

### Author contributions

I.B. and L.M. have contributed equally to this work. G.D.L., C.B.E., A.D., L.G., A.E., S.J. and M.G. grew and characterized the  $\text{La}_2\text{NiO}_4$  films. I.B., J.Choi, M.G.-F., S.A., K.-J.Z, K.K., N.B.B. and Q.W. carried out the RIXS experiments. I.B., L.M. and Q.W. analysed the RIXS data. P.W., J.M.T and K.H. conceived, executed and analysed the *ab initio* calculations. I.B., Q.W. and J.C. conceived the project. All authors contributed to the writing of the manuscript.

### Acknowledgements

I.B. and L.M. acknowledge support from the Swiss Government Excellence Scholarship under project numbers ESKAS-Nr: 2022.0001 and ESKAS-Nr: 2023.0052. G.D.L, M.G. and J.C. thank the Swiss National Science Foundation under Projects No. 200021\_188564 and PP00P2\_170564. Q.W. is supported by the Research Grants Council of Hong Kong (ECS No. 24306223), and the CUHK Direct Grant (No. 4053613). G.D.L. acknowledges support from the UZH GRC Travel Grant. We acknowledge Diamond Light Source for providing beam time on beamline I21 under Proposal MM30189 and the European Synchrotron Radiation Facility (ESRF) for providing beam time on beamline ID32 under Proposal HC 5241. C.B.E. acknowledges support for this research through a Vannevar Bush Faculty Fellowship (ONR N00014-20-1-2844), the Gordon and Betty Moore Foundation's EPiQS Initiative, Grant GBMF9065 and NSF through the University of Wisconsin Materials Research Science and Engineering Center (DMR-2309000). The synthesis of thin films at the University of Wisconsin-Madison was supported by the US Department of Energy (DOE), Office of Science, Office of Basic Energy Sciences (BES), under award number DE-FG02-06ER46327.

### Competing interests

The authors declare that they have no competing interests.

## REFERENCES

- [1] P. A. Lee, N. Nagaosa, and X.-G. Wen, Doping a Mott insulator: Physics of high-temperature superconductivity, *Rev. Mod. Phys.* **78**, 17 (2006).
- [2] N. B. Christensen, H. M. Rønnow, D. F. McMorrow, A. Harrison, T. G. Perring, M. Enderle, R. Coldea, L. P. Regnault, and G. Aeppli, Quantum dynamics and entanglement of spins on a square lattice, *PNAS* **104**, 15264 (2007).
- [3] N. S. Headings, S. M. Hayden, R. Coldea, and T. G. Perring, Anomalous High-Energy Spin Excitations in the High- $T_c$  Superconductor-Parent Antiferromagnet  $\text{La}_2\text{CuO}_4$ , *Phys. Rev. Lett.* **105**, 247001 (2010).
- [4] R. Coldea, S. M. Hayden, G. Aeppli, T. G. Perring, C. D. Frost, T. E. Mason, S.-W. Cheong, and Z. Fisk, Spin waves and electronic interactions in  $\text{La}_2\text{CuO}_4$ , *Phys. Rev. Lett.* **86**, 5377 (2001).
- [5] K. Choo, T. Neupert, and G. Carleo, Two-dimensional frustrated  $J_1-J_2$  model studied with neural network quantum states, *Phys. Rev. B* **100**, 125124 (2019).
- [6] L. Capriotti and S. Sorella, Spontaneous plaquette dimerization in the  $J_1-J_2$  Heisenberg model, *Phys. Rev. Lett.* **84**, 3173 (2000).
- [7] L. Capriotti, F. Becca, A. Parola, and S. Sorella, Resonating valence bond wave functions for strongly frustrated spin systems, *Phys. Rev. Lett.* **87**, 097201 (2001).
- [8] G.-M. Zhang, H. Hu, and L. Yu, Valence-bond spin-liquid state in two-dimensional frustrated spin-1/2 Heisenberg antiferromagnets, *Phys. Rev. Lett.* **91**, 067201 (2003).
- [9] S.-S. Gong, W. Zhu, D. N. Sheng, O. I. Motrunich, and M. P. A. Fisher, Plaquette ordered phase and quantum phase diagram in the spin- $\frac{1}{2}$   $J_1-J_2$  square Heisenberg model, *Phys. Rev. Lett.* **113**, 027201 (2014).
- [10] O. P. Sushkov, J. Oitmaa, and Z. Weihong, Quantum phase transitions in the two-dimensional  $J_1-J_2$  model, *Phys. Rev. B* **63**, 104420 (2001).
- [11] H. C. Jiang, F. Krüger, J. E. Moore, D. N. Sheng, J. Zanen, and Z. Y. Weng, Phase diagram of the frustrated spatially-anisotropic  $S=1$  antiferromagnet on a square lattice, *Phys. Rev. B* **79**, 174409 (2009).
- [12] P. W. Anderson, The Resonating Valence Bond State in  $\text{La}_2\text{CuO}_4$  and Superconductivity, *Science* **235**, 1196 (1987).
- [13] E. Dagotto and A. Moreo, Phase diagram of the frustrated spin-1/2 Heisenberg antiferromagnet in 2 dimensions, *Phys. Rev. Lett.* **63**, 2148 (1989).
- [14] H. J. Schulz, T. A. Ziman, and D. Poilblanc, Magnetic order and disorder in the frustrated quantum Heisenberg antiferromagnet in two dimensions, *Journal de Physique I* **6**, 675-703 (1996).
- [15] K. S. D. Beach, Master equation approach to computing RVB bond amplitudes, *Phys. Rev. B* **79**, 224431 (2009).
- [16] Q. Wang, Y. Shen, B. Pan, X. Zhang, K. Ikeuchi, K. Iida, A. D. Christianson, H. C. Walker, D. T. Adroja, M. Abdel-Hafez, X. Chen, D. A. Chareev, A. N. Vasiliev, and J. Zhao, Magnetic ground state of FeSe, *Nat. Commun.* **7**, 12182 (2016).
- [17] Y. Gu, Q. Wang, H. Wo, Z. He, H. C. Walker, J. T. Park, M. Enderle, A. D. Christianson, W. Wang, and J. Zhao, Frustrated magnetic interactions in FeSe, *Phys. Rev. B* **106**, L060504 (2022).
- [18] O. Mustonen, S. Vasala, E. Sadrollahi, K. P. Schmidt, C. Baines, H. C. Walker, I. Terasaki, F. J. Litterst, E. Baggio-Saitovitch, and M. Karppinen, Spin-liquid-like state in a spin-1/2 square-lattice antiferromagnet perovskite induced by  $d^{10}-d^0$  cation mixing, *Nat. Commun.* **9**, 1085 (2018).
- [19] O. Ivashko, M. Horio, W. Wan, N. B. Christensen, D. E. McNally, E. Paris, Y. Tseng, N. E. Shaik, H. M. Rønnow, H. I. Wei, C. Adamo, C. Lichtensteiger, M. Gibert, M. R. Beasley, K. M. Shen, J. M. Tomczak, T. Schmitt, and J. Chang, Strain-engineering Mott-insulating  $\text{La}_2\text{CuO}_4$ , *Nat. Commun.* **10**, 786 (2019).

- [20] J. Goodenough and S. Ramasesha, Further evidence for the coexistence of localized and itinerant  $3d$  electrons in  $\text{La}_2\text{NiO}_4$ , *Materials Research Bulletin* **17**, 383 (1982).
- [21] P. G. Radaelli, D. G. Hinks, A. W. Mitchell, B. A. Hunter, J. L. Wagner, B. Dabrowski, K. G. Vandervoort, H. K. Viswanathan, and J. D. Jorgensen, Structural and superconducting properties of  $\text{La}_{2-x}\text{Sr}_x\text{CuO}_4$  as a function of Sr content, *Phys. Rev. B* **49**, 4163 (1994).
- [22] A. Nag, H. C. Robarts, F. Wenzel, J. Li, H. Elnaggar, R.-P. Wang, A. C. Walters, M. García-Fernández, F. M. F. de Groot, M. W. Haverkort, and K.-J. Zhou, Many-body physics of single and double spin-flip excitations in NiO, *Phys. Rev. Lett.* **124**, 067202 (2020).
- [23] G. Ghiringhelli, M. Matsubara, C. Dallera, F. Fracassi, R. Gusmeroli, A. Piazzalunga, A. Tagliaferri, N. B. Brookes, A. Kotani, and L. Braicovich, NiO as a test case for high resolution resonant inelastic soft x-ray scattering, *J. Phys.: Condens. Matter* **17**, 5397 (2005).
- [24] J. Q. Lin, P. Villar Arribi, G. Fabbri, A. S. Botana, D. Meyers, H. Miao, Y. Shen, D. G. Mazzone, J. Feng, S. G. Chiuzbaian, A. Nag, A. C. Walters, M. García-Fernández, K.-J. Zhou, J. Pelliciari, I. Jarrige, J. W. Freeland, J. Zhang, J. F. Mitchell, V. Bisogni, X. Liu, M. R. Norman, and M. P. M. Dean, Strong superexchange in a  $d^{9-\delta}$  nickelate revealed by resonant inelastic x-ray scattering, *Phys. Rev. Lett.* **126**, 087001 (2021).
- [25] P. Kuiper, J. van Elp, D. E. Rice, D. J. Buttrey, H.-J. Lin, and C. T. Chen, Polarization-dependent nickel  $2p$  x-ray-absorption spectra of  $\text{La}_2\text{NiO}_{4+\delta}$ , *Phys. Rev. B* **57**, 1552 (1998).
- [26] G. Ghiringhelli, A. Piazzalunga, C. Dallera, T. Schmitt, V. N. Strocov, J. Schlappa, L. Patthey, X. Wang, H. Berger, and M. Grioni, Observation of Two Nondispersive Magnetic Excitations in NiO by Resonant Inelastic Soft-X-Ray Scattering, *Phys. Rev. Lett.* **102**, 027401 (2009).
- [27] G. Fabbri, D. Meyers, L. Xu, V. M. Katukuri, L. Hozoi, X. Liu, Z.-Y. Chen, J. Okamoto, T. Schmitt, A. Uldry, B. Delley, G. D. Gu, D. Prabhakaran, A. T. Boothroyd, J. van den Brink, D. J. Huang, and M. P. M. Dean, Doping Dependence of Collective Spin and Orbital Excitations in the Spin-1 Quantum Antiferromagnet  $\text{La}_{2-x}\text{Sr}_x\text{NiO}_4$  Observed by X Rays, *Phys. Rev. Lett.* **118**, 156402 (2017).
- [28] L. Pintschovius, J. M. Bassat, P. Odier, F. Gervais, G. Chevrier, W. Reichardt, and F. Gompf, Lattice dynamics of  $\text{La}_2\text{NiO}_4$ , *Phys. Rev. B* **40**, 2229 (1989).
- [29] L. Pintschovius, J.-M. Bassat, P. Odier, F. Gervais, B. Hennion, and W. Reichardt, Phonon Anomalies in  $\text{La}_2\text{NiO}_4$ , *Europhysics Letters* **5**, 247 (1988).
- [30] K. Nakajima, K. Yamada, S. Hosoya, T. Omata, and Y. Endoh, Spin-Wave Excitations in Two Dimensional Antiferromagnet of Stoichiometric  $\text{La}_2\text{NiO}_4$ , *Journal of the Physical Society of Japan* **62**, 4438–4448 (1993).
- [31] A. N. Petsch, N. S. Headings, D. Prabhakaran, A. I. Kolesnikov, C. D. Frost, A. T. Boothroyd, R. Coldea, and S. M. Hayden, High-energy spin waves in the spin-1 square-lattice antiferromagnet  $\text{La}_2\text{NiO}_4$ , *Phys. Rev. Res.* **5**, 033113 (2023).
- [32] Y. Y. Peng, G. Dellea, M. Minola, M. Conni, A. Amorese, D. Di Castro, G. M. De Luca, K. Kummer, M. Saluzzo, X. Sun, X. J. Zhou, G. Balestrino, M. Le Tacon, B. Keimer, L. Braicovich, N. B. Brookes, and G. Ghiringhelli, Influence of apical oxygen on the extent of in-plane exchange interaction in cuprate superconductors, *Nature Phys.* **13**, 1201–1206 (2017).
- [33] O. Ivashko, N. E. Shaik, X. Lu, C. G. Fatuzzo, M. Dantz, P. G. Freeman, D. E. McNally, D. Destraz, N. B. Christensen, T. Kurosawa, N. Momono, M. Oda, C. E. Matt, C. Monney, H. M. Rønnow, T. Schmitt, and J. Chang, Damped spin excitations in a doped cuprate superconductor with orbital hybridization, *Phys. Rev. B* **95**, 214508 (2017).
- [34] G. Aeppli and D. J. Buttrey, Magnetic Correlations in  $\text{La}_2\text{NiO}_{4+\delta}$ , *Phys. Rev. Lett.* **61**, 203 (1988).
- [35] K. Yamada, T. Omata, K. Nakajima, S. Hosoya, T. Sumida, and Y. Endoh, Magnetic structure and weak ferromagnetism of  $\text{La}_2\text{NiO}_{4+\delta}$ , *Physica C: Superconductivity* **191**, 15 (1992).
- [36] J. Rodriguez-Carvajal, M. T. Fernandez-Diaz, and J. L. Martinez, Neutron diffraction study on structural and magnetic properties of  $\text{La}_2\text{NiO}_4$ , *J. Phys.: Condens. Matter* **3**, 3215 (1991).
- [37] K. Yamada, M. Arai, Y. Endoh, S. Hosoya, K. Nakajima, T. Perring, and A. Taylor, Complete Two-Dimensional Antiferromagnetic Spin-Wave Dispersion Relation of  $\text{La}_2\text{NiO}_4$  Determined by Chopper Spectrometer Installed at the Pulsed Neutron Source, *J. Phys. Soc. Jpn.* **60**, 1197 (1991).
- [38] J. Igarashi,  $1/S$  expansion for thermodynamic quantities in a two-dimensional Heisenberg antiferromagnet at zero temperature, *Phys. Rev. B* **46**, 10763 (1992).
- [39] H. Lu, M. Rossi, A. Nag, M. Osada, D. F. Li, K. Lee, B. Y. Wang, M. Garcia-Fernandez, S. Agrestini, Z. X. Shen, E. M. Been, B. Moritz, T. P. Devereaux, J. Zaanen, H. Y. Hwang, K.-J. Zhou, and W. S. Lee, Magnetic excitations in infinite-layer nickelates, *Science* **373**, 213 (2021).
- [40] Q. Gao, S. Fan, Q. Wang, J. Li, X. Ren, I. Bialo, A. Drewanowski, P. Rothenbühler, J. Choi, R. Sutarto, Y. Wang, T. Xiang, J. Hu, K.-J. Zhou, V. Bisogni, R. Comin, J. Chang, J. Pelliciari, X. J. Zhou, and Z. Zhu, Magnetic excitations in strained infinite-layer nickelate  $\text{prnio2}$  films, *Nature Communications* **15**, 10.1038/s41467-024-49940-4 (2024).
- [41] J.-Y. P. Delannoy, M. J. P. Gingras, P. C. W. Holdsworth, and A.-M. S. Tremblay, Low-energy theory of the  $t - t' - t'' - U$  Hubbard model at half-filling: Interaction strengths in cuprate superconductors and an effective spin-only description of  $\text{La}_2\text{CuO}_4$ , *Phys. Rev. B* **79**, 235130 (2009).
- [42] B. Dalla Piazza, M. Mourigal, M. Guarise, H. Berger, T. Schmitt, K. J. Zhou, M. Grioni, and H. M. Rønnow, Unified one-band hubbard model for magnetic and electronic spectra of the parent compounds of cuprate superconductors, *Phys. Rev. B* **85**, 100508 (2012).
- [43] M. Horio, C. E. Matt, K. Kramer, D. Sutter, A. M. Cook, Y. Sassa, K. Hauser, M. Månsson, N. C. Plumb, M. Shi, O. J. Lipscombe, S. M. Hayden, T. Neupert, and J. Chang, Two-dimensional type-II Dirac fermions in layered oxides, *Nat. Commun.* **9**, 3252 (2018).
- [44] M. Uchida, K. Ishizaka, P. Hansmann, X. Yang, M. Sakano, J. Miyawaki, R. Arita, Y. Kaneko, Y. Takata, M. Oura, A. Toschi, K. Held, A. Chainani, O. K. Andersen, S. Shin, and Y. Tokura, Orbital characters of three-dimensional Fermi surfaces in  $\text{Eu}_{2-x}\text{Sr}_x\text{NiO}_4$  as probed by soft-x-ray angle-resolved photoemission spectroscopy,



Phys. Rev. B **84**, 241109 (2011).

- [45] M. Uchida, K. Ishizaka, P. Hansmann, Y. Kaneko, Y. Ishida, X. Yang, R. Kumai, A. Toschi, Y. Onose, R. Arita, K. Held, O. K. Andersen, S. Shin, and Y. Tokura, Pseudogap of Metallic Layered Nickelate  $R_{2-x}\text{Sr}_x\text{NiO}_4$  ( $R = \text{Nd, Eu}$ ) Crystals Measured Using Angle-Resolved Photoemission Spectroscopy, *Phys. Rev. Lett.* **106**, 027001 (2011).
- [46] C. E. Matt, D. Sutter, A. M. Cook, Y. Sassa, M. Månsson, O. Tjernberg, L. Das, M. Horio, D. De-straz, C. G. Fatuzzo, K. Hauser, M. Shi, M. Kobayashi, V. N. Strocov, T. Schmitt, P. Dudin, M. Hoesch, S. Pyon, T. Takayama, H. Takagi, O. J. Lipscombe, S. M. Hayden, T. Kurosawa, N. Momono, M. Oda, T. Neupert, and J. Chang, Direct observation of orbital hybridisation in a cuprate superconductor, *Nat. Commun.* **9**, 972 (2018).
- [47] J. M. Tomczak, T. Miyake, R. Sakuma, and F. Aryasetiawan, Effective Coulomb interactions in solids under pressure, *Phys. Rev. B* **79**, 235133 (2009).
- [48] R. Lemanski and J. Matysiak, Two-orbital Hubbard model vs spin  $S = 1$  Heisenberg model: Studies on clusters, *Condensed Matter Physics* **21**, 33301 (2018).
- [49] F. Aryasetiawan, M. Imada, A. Georges, G. Kotliar, S. Biermann, and A. I. Lichtenstein, Frequency-dependent local interactions and low-energy effective models from electronic structure calculations, *Phys. Rev. B* **70**, 195104 (2004).
- [50] A. H. MacDonald, S. M. Girvin, and D. Yoshioka, Reply to “Comment on ‘t/U expansion for the Hubbard model’”, *Phys. Rev. B* **41**, 2565 (1990).
- [51] J. P. Podkaminer, J. J. Patzner, B. A. Davidson, and C. B. Eom, Real-time and *in situ* monitoring of sputter deposition with RHEED for atomic layer controlled growth, *APL Materials* **4**, 086111 (2016).
- [52] K.-J. Zhou, A. Walters, M. Garcia-Fernandez, T. Rice, M. Hand, A. Nag, J. Li, S. Agrestini, P. Garland, H. Wang, S. Alcock, I. Nistea, B. Nutter, N. Rubies, G. Knap, M. Gaughran, F. Yuan, P. Chang, J. Emmins, and G. Howell, I21: an advanced high-resolution resonant inelastic X-ray scattering beamline at Diamond Light Source, *J. Synchrotron Rad.* **29**, 563 (2022).
- [53] Q. Wang, M. Horio, K. von Arx, Y. Shen, D. John Mukkattukavil, Y. Sassa, O. Ivashko, C. E. Matt, S. Pyon, T. Takayama, H. Takagi, T. Kurosawa, N. Momono, M. Oda, T. Adachi, S. M. Haidar, Y. Koike, Y. Tseng, W. Zhang, J. Zhao, K. Kummer, M. Garcia-Fernandez, K.-J. Zhou, N. B. Christensen, H. M. Rønnow, T. Schmitt, and J. Chang, High-temperature charge-stripe correlations in  $\text{La}_{1.675}\text{Eu}_{0.2}\text{Sr}_{0.125}\text{CuO}_4$ , *Phys. Rev. Lett.* **124**, 187002 (2020).
- [54] S. Toth and B. Lake, Linear spin wave theory for single-Q incommensurate magnetic structures, *Journal of Physics: Condensed Matter* **27**, 166002 (2015).
- [55] M. Methfessel, M. van Schilfgaarde, and R. Casali, A full-potential lmto method based on smooth hankel functions, in *Electronic Structure and Physical Properties of Solids: The Uses of the LMTO Method*, Lecture Notes in Physics. H. Dreysse, ed. **535** (2000).
- [56] P. Blaha, K. Schwarz, F. Tran, R. Laskowski, G. K. H. Madsen, and L. D. Marks, WIEN2k: An APW+lo program for calculating the properties of solids, *J. Chem. Phys.* **152**, 074101 (2020).
- [57] N. Marzari, A. A. Mostofi, J. R. Yates, I. Souza, and D. Vanderbilt, Maximally localized Wannier functions: Theory and applications, *Rev. Mod. Phys.* **84**, 1419 (2012).
- [58] T. Miyake and F. Aryasetiawan, Screened Coulomb interaction in the maximally localized Wannier basis, *Phys. Rev. B* **77**, 085122 (2008).
- [59] T. Miyake, F. Aryasetiawan, and M. Imada, *Ab initio* procedure for constructing effective models of correlated materials with entangled band structure, *Phys. Rev. B* **80**, 155134 (2009).

# Supplementary Information: Strain-Tuned Incompatible Magnetic Exchange-Interaction in $\text{La}_2\text{NiO}_4$

Izabela Bialo,<sup>1,2,\*</sup> Leonardo Martinelli,<sup>1</sup> Gabriele De Luca,<sup>3</sup> Paul Worm,<sup>4</sup> Annabella Drewanowski,<sup>1</sup> Simon Jöhr,<sup>1</sup> Jaewon Choi,<sup>5</sup> Mirian Garcia-Fernandez,<sup>5</sup> Stefano Agrestini,<sup>5</sup> Ke-Jin Zhou,<sup>5</sup> Kurt Kummer,<sup>6</sup> Nicholas B. Brookes,<sup>6</sup> Luo Guo,<sup>7</sup> Anthony Edgeton,<sup>7</sup> Chang B. Eom,<sup>7</sup> Jan M. Tomczak,<sup>8,4</sup> Karsten Held,<sup>4</sup> Marta Gibert,<sup>4</sup> Qisi Wang,<sup>9,1,†</sup> and Johan Chang<sup>1</sup>

<sup>1</sup>*Physik-Institut, Universität Zürich, Winterthurerstrasse 190, CH-8057 Zürich, Switzerland*

<sup>2</sup>*AGH University of Krakow, Faculty of Physics and Applied Computer Science, 30-059 Krakow, Poland*

<sup>3</sup>*Institut de Ciència de Materials de Barcelona (ICMAB-CSIC), 08193 Bellaterra (Barcelona), Spain*

<sup>4</sup>*Institute of Solid State Physics, Vienna University of Technology, A-1040 Vienna, Austria*

<sup>5</sup>*Diamond Light Source, Harwell Campus, Didcot, Oxfordshire OX11 0DE, United Kingdom*

<sup>6</sup>*ESRF, The European Synchrotron, 71 Avenue des Martyrs, CS40220, 38043 Grenoble Cedex 9, France*

<sup>7</sup>*Department of Materials Science and Engineering, University of Wisconsin-Madison, Madison, 53706, Wisconsin, USA*

<sup>8</sup>*Department of Physics, King's College London, Strand, London WC2R 2LS, United Kingdom*

<sup>9</sup>*Department of Physics, The Chinese University of Hong Kong, Shatin, Hong Kong, China*

## SUPPLEMENTARY NOTE 1: CRYSTAL FIELD CHARACTERISTIC

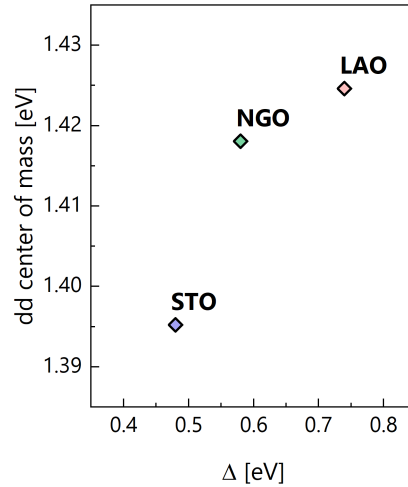


FIG. S1. **Crystal field splitting of  $\text{La}_2\text{NiO}_4$  films.** Crystal field splitting ( $\Delta$ ) of  $\text{La}_2\text{NiO}_4$  (LNO) films grown on different substrates, by which the Ni  $d_{x^2-y^2}$  orbital is higher in energy than the  $d_{z^2}$  orbital.  $\Delta$  is calculated by DFT and compared with the center of mass of the  $dd$  excitations, for samples as indicated (SrTiO<sub>3</sub> (STO), LaAlO<sub>3</sub> (LAO), and NdGaO<sub>3</sub> (NGO)).

\* izabela.bialo@uzh.ch

† qwang@cuhk.edu.hk

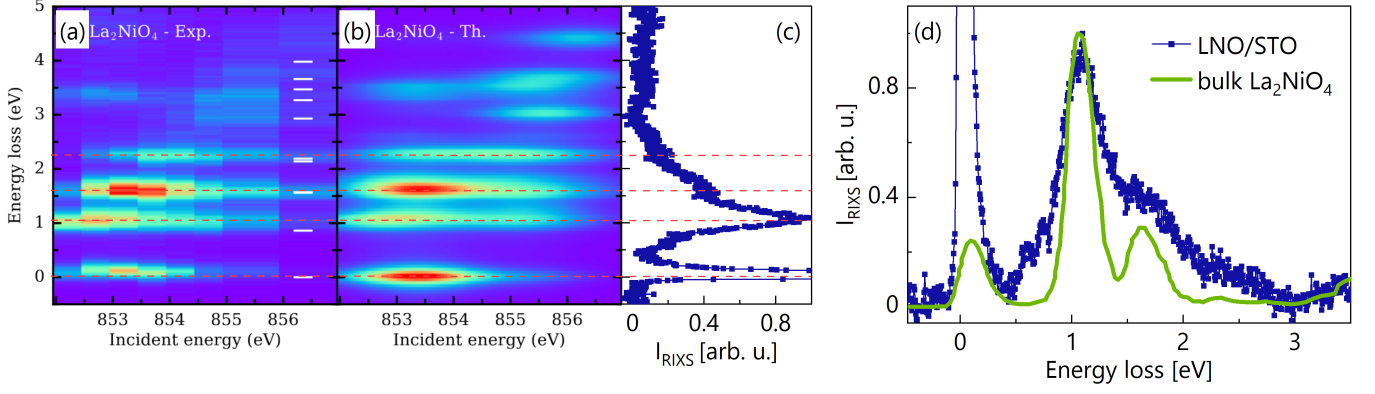


FIG. S2. **Comparison of Ni L<sub>3</sub>-edge resonant inelastic x-ray scattering spectra between LNO films and existing literature data.** (a) Resonant inelastic x-ray scattering (RIXS) energy map of the bulk La<sub>2</sub>NiO<sub>4</sub>. White bars shows relative energies as computed by multireference configuration-interaction. Adapted from [1] with permission. (b) Corresponding Ni L<sub>3</sub>-edge RIXS atomic multiplet calculations. Pink lines are guides-to-the-eye, indicating the main crystal field features, present both in experimental and theoretical spectra. Adapted from [1] with permission. (c) RIXS spectrum of LNO/STO film. (d) RIXS spectra collected for LNO/STO and for bulk La<sub>2</sub>NiO<sub>4</sub>.

#### SUPPLEMENTARY NOTE 2: EXCHANGE INTERACTIONS DERIVED FROM EXPERIMENTAL DATA

System	$J_1^{exp}$ [meV]	$J_1^{exp}$ error [meV]	$J_2^{exp}$ [meV]	$J_2^{exp}$ error [meV]
bulk La <sub>2</sub> NiO <sub>4</sub>	28.59	1.17	1.47	0.74
LNO/STO	26.38	1.53	3.23	1.26
LNO/LSAT	30.23	1.85	5.14	1.34
LNO/NGO	30.75	0.70	4.35	0.54
LNO/LAO	34.12	1.27	6.95	0.80

TABLE S1. **Experimental values of the effective exchange interactions.** The effective nearest-neighbor ( $J_1^{exp}$ ) and the next-nearest-neighbour interactions ( $J_2^{exp}$ ) calculated based on the spin-wave model, where  $E_X = 4SZ_c(J_1 - 2J_2)$  and  $E_\Sigma = 4SZ_c(J_1 - J_2)$ .  $E_\Sigma$  refers to the magnon energy at the  $\Sigma$  point ( $1/4, 1/4$ ), while  $E_X$  represents the magnon energy in the  $X$  point ( $1/2, 0$ ). The quantum renormalization factor for spin-wave velocity is fixed to  $Z_c = 1.09$ , as usual for  $S = 1$  systems [2]. The error bars for the experimental data are calculated as a propagation of standard deviations extracted from the fits of RIXS spectra. LSAT stands for the (LaAlO<sub>3</sub>)<sub>0.3</sub>(Sr<sub>2</sub>TaAlO<sub>6</sub>)<sub>0.7</sub> substrate.

#### SUPPLEMENTARY NOTE 3: DERIVING THE EXCHANGE INTERACTION FROM DFT AND CRPA

In this section, we provide further details on how to arrive at the exchange coupling Eq. (1) of the main text, starting from the DFT Wannier Hamiltonian and the cRPA calculated interactions. The Wannier projection maps the DFT bandstructure onto two low-energy  $e_g$  bands with the Hamiltonian of a two-orbital Hubbard model

$$\begin{aligned}
\mathcal{H} = & \sum_{ijmm'\sigma} t_{ijmm'} c_{im\sigma}^\dagger c_{jm'\sigma} + \Delta \sum_{i\sigma} n_{i\beta\sigma} + U \sum_{i,m} n_{im\uparrow} n_{im\downarrow} + \sum_{i\sigma\sigma'} (U' - \delta_{\sigma\sigma'} J_H) n_{i\alpha\sigma} n_{i\beta\sigma'} \\
& - J_H \sum_{im} (c_{im\downarrow}^\dagger c_{i\bar{m}\uparrow}^\dagger c_{i\bar{m}\downarrow} c_{im\uparrow} + c_{im\downarrow}^\dagger c_{im\uparrow}^\dagger c_{i\bar{m}\downarrow} c_{i\bar{m}\uparrow})
\end{aligned} \tag{1}$$

Here,  $c_{im\sigma}^\dagger$  ( $c_{im\sigma}$ ) creates (annihilates) an electron with spin  $\sigma \in \{\uparrow, \downarrow\}$  on site  $i$  in orbital  $m \in \{\alpha, \beta\}$  denoting the two  $e_g$  orbitals;  $n_{im\sigma} = c_{im\sigma}^\dagger c_{im\sigma}$  is the occupation number operator for said state and  $\bar{\sigma}$  ( $\bar{m}$ ) the spin (orbital) opposite to  $\sigma$  ( $m$ ). The DFT part consists of the hopping elements  $t_{ijmm'}$  and the crystal field splitting  $\Delta$  between the two orbitals; the cRPA calculated intra-orbital Hubbard interaction is denoted by  $U$ ,  $J_H$  is the local Hund's exchange and pair hopping, and  $U' = U - 2J$  the intra-orbital interaction. All the parameters are listed in Table I of the main text.

If we now consider the atomic limit ( $t \rightarrow 0$ ), half-filling of the  $e_g$  orbitals and the case  $J_H > \Delta$ , two electrons on each site will form a local spin-1. From this starting point we can next include  $t$  in second order perturbation theory. That is, we start with an arrangement of spins, let one electron on site  $i$  hop to another site  $j$  with a hopping amplitude  $t_{ijmm'}$  (forming an excited state) and hop back. This leads to an energy gain depending on the relative arrangement of the spins on the sites  $i$  and  $j$ , that can be described by an effective spin-1 Heisenberg model:

$$H = \frac{1}{2} \sum_{i,j} J_{ij} \mathbf{S}_i \mathbf{S}_j, \quad (2)$$

where  $\mathbf{S}_i$  is the spin-1 operator on site  $i$  and the factor  $1/2$  corrects for the fact that each pair of sites is counted twice in the sum.

The value of  $J_{ij}$  depends on the energy gain of the virtual hopping process. As it only involves two sites (in second order perturbation theory), we only need to consider the two-site version of the two Hamiltonians Eq. (1) and Eq. (2). Given the mapping onto a Heisenberg model with SU(2) symmetry, we can then calculate  $J_{ij}$  from considering any two spin configurations of these two sites  $i = 1$  and  $j = 2$ .

For the sake of simplicity, one spin state which we consider is the one with maximal spin:

$$|S = 2, S_z = +2\rangle = c_{i\alpha\uparrow}^\dagger c_{i\beta\uparrow}^\dagger c_{j\alpha\uparrow}^\dagger c_{j\beta\uparrow}^\dagger |0\rangle. \quad (3)$$

It is particularly simple, as no hopping is possible and its energy is simply twice the ground-state energy of the atomic limit of Eq. (1):  $E_0 = 2(U - 3J_H + \Delta)$ . The second spin configuration that we consider is

$$|S = 1, S_z = 0\rangle = \frac{1}{\sqrt{2}} \left( c_{i\alpha\uparrow}^\dagger c_{i\beta\uparrow}^\dagger c_{j\alpha\downarrow}^\dagger c_{j\beta\downarrow}^\dagger - c_{i\alpha\downarrow}^\dagger c_{i\beta\downarrow}^\dagger c_{j\alpha\uparrow}^\dagger c_{j\beta\uparrow}^\dagger \right). \quad (4)$$

Its energy in second order perturbation theory is

$$E = E_0 + \sum_k \frac{|\langle k | H_t | S = 1, S_z = 0 \rangle|^2}{(E_0 - E_k)} \quad (5)$$

where  $H_t$  is the first (hopping) term of Hamiltonian Eq. (1). After some algebra for the sum over the excited states  $k$ , we obtain

$$E = E_0 - 2 \left( \frac{t_{ij\alpha\beta}^2}{U + J_H - \Delta} + \frac{t_{ijj\alpha\beta}^2}{U + J_H + \Delta} + \frac{t_{ij\alpha\alpha}^2 + t_{ij\beta\beta}^2}{U + J_H} \right). \quad (6)$$

The spin-1 Heisenberg model has, on the other hand, total energy  $E = J_{ij}$  and  $E = -J_{ij}$  for the configuration Eq. (3) and Eq. (4), respectively. Requiring the same energy difference,  $E - E_0$ , then yields Eq. (1) of the main text. In the main text, we have relabeled  $J_{ij}$  as  $J_1^{\text{cal}}$  and  $J_2^{\text{cal}}$  depending on whether  $i$  and  $j$  are the nearest or the next-nearest neighbors.



# SUPPLEMENTARY NOTE 4: RESISTIVITY MEASUREMENTS

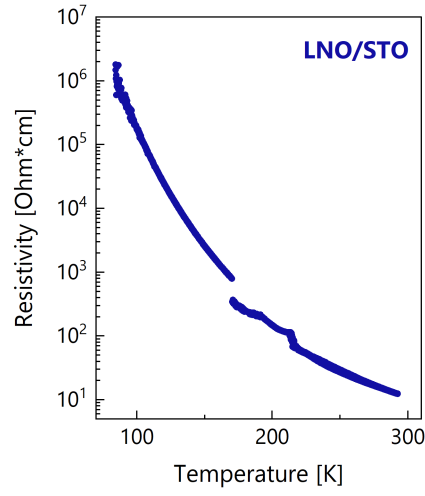


FIG. S3. **Resistivity of the LNO/STO plotted in logarithmic scale versus temperature.** Resistivity decreases with increasing temperature, indicating an insulating character of the sample. Measurements were taken while warming from 100 to 300 K.

# SUPPLEMENTARY NOTE 5: RIXS SPECTRA OF LNO/LSAT FILMS

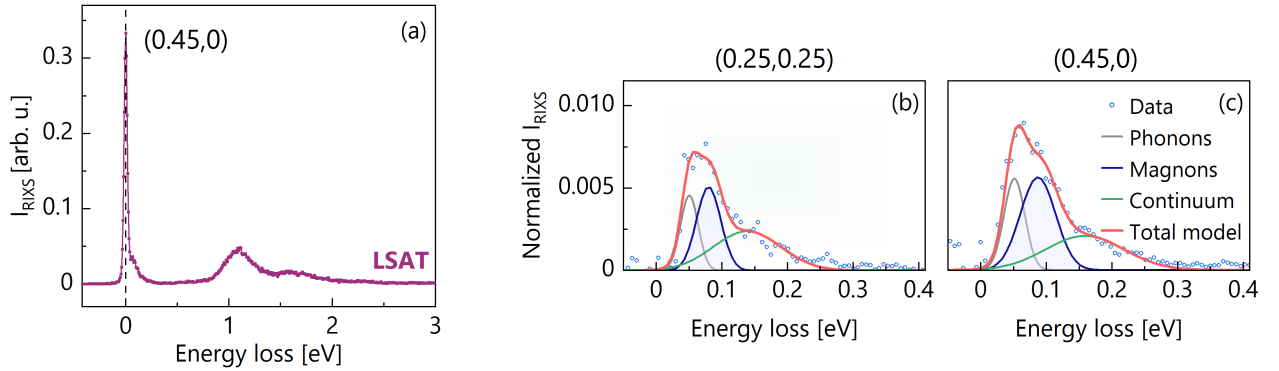


FIG. S4. **Experimental data for LNO/LSAT films.** (a) Raw RIXS spectra measured at 25 K at the ID32 beamline, at ESRF synchrotron. (b,c) Low energy part of the RIXS spectra. The solid red line indicates a three-component Gaussian fit to normalized data with phonon, magnon (shaded), and multi-magnon (continuum) contributions. The elastic scattering channel is subtracted. The subtracted elastic peak was fitted by an asymmetric pseudo-voigt function, with fitting parameters estimated from the elastic scattering on silver paint. The experimental resolution was estimated as  $\sim 31$  meV. (a-c) In-plane momentum transfers are indicated.

**SUPPLEMENTARY NOTE 6: BAND-STRUCTURE OF  $\text{La}_2\text{NiO}_4$**

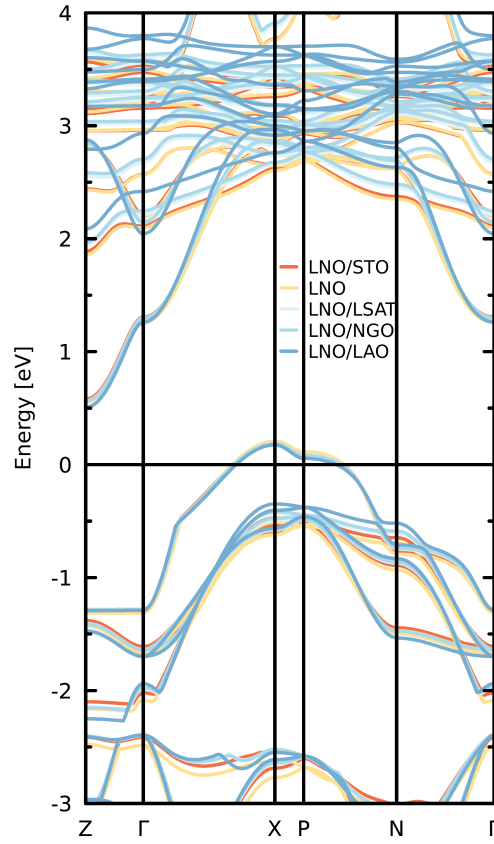


FIG. S5. **Band structure calculations for  $\text{La}_2\text{NiO}_4$  grown on a different substrates.** Shown are the DFT-bands obtained from (tetragonal) bulk calculations that use the experimental lattice constants of the various thin films. The color code indicates the considered substrate. The yellow lines (LNO) refer to bulk conditions.

**SUPPLEMENTARY NOTE 7: THE STRUCTURAL DATA AFTER DFT RELAXATION**

System	$a$ [Å]	$c$ [Å]	O(00z)/ $c$ [-]	O(00z) [Å]	La(00z)/ $c$ [-]	La (00z) [Å]
bulk $\text{La}_2\text{NiO}_4$	3.890	12.55	0.179	2.250	0.364	4.562
LNO/STO	3.905	12.62	0.180	2.271	0.363	4.586
LNO/LSAT	3.868	12.69	0.180	2.286	0.363	4.610
LNO/NGO	3.859	12.71	0.180	2.292	0.363	4.616
LNO/LAO	3.793	12.78	0.181	2.312	0.363	4.636

TABLE S2. **Positions of selected ions obtained from structure optimizations for different lattice constants.** In this convention, the Ni atom stays in (000) position. The relative distances within the unit cell are not substantially different between different substrates. The electronic structure evolves mainly due to changes of  $c$ -axis length.

## SUPPLEMENTARY REFERENCES

- [1] G. Fabbri, D. Meyers, L. Xu, V. M. Katukuri, L. Hozoi, X. Liu, Z.-Y. Chen, J. Okamoto, T. Schmitt, A. Uldry, B. Delley, G. D. Gu, D. Prabhakaran, A. T. Boothroyd, J. van den Brink, D. J. Huang, and M. P. M. Dean, Doping Dependence of Collective Spin and Orbital Excitations in the Spin-1 Quantum Antiferromagnet  $\text{La}_{2-x}\text{Sr}_x\text{NiO}_4$  Observed by X Rays, [Phys. Rev. Lett.](#) **118**, 156402 (2017).
- [2] J. Igarashi,  $1/S$  expansion for thermodynamic quantities in a two-dimensional Heisenberg antiferromagnet at zero temperature, [Phys. Rev. B](#) **46**, 10763 (1992).